

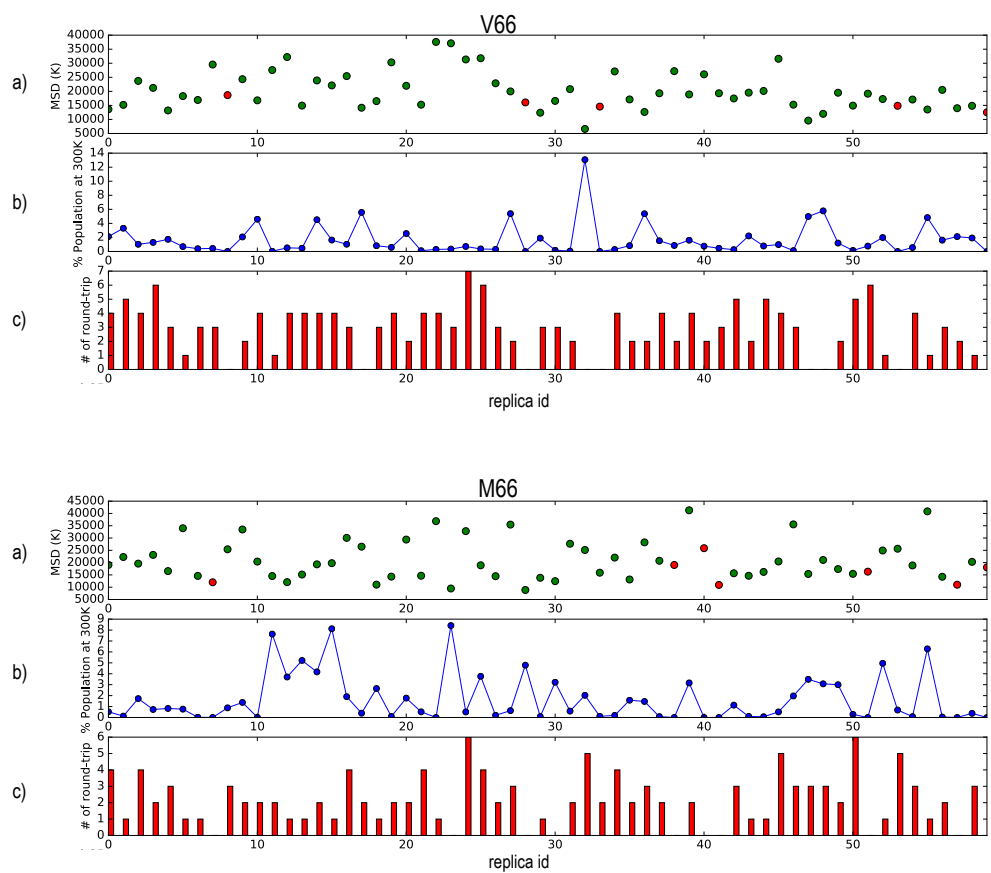
Mechanism underlying conformational effects of a disease-associated hydrophobic-to-hydrophobic substitution on an intrinsically disordered region

Ruchi Lohia¹, Reza Salari¹, Grace Brannigan^{1,2*},

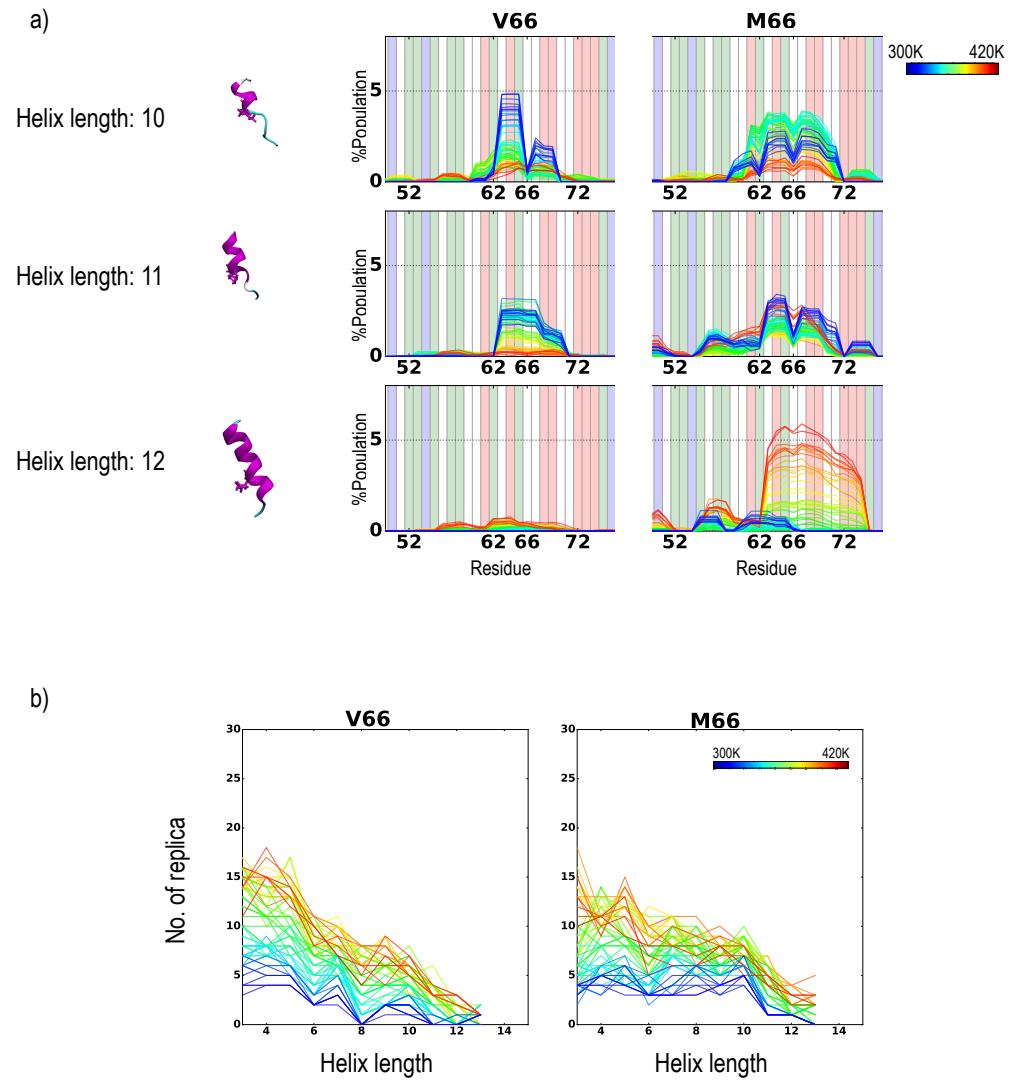
1 Center for Computational and Integrative Biology, Rutgers University, Camden, NJ, USA

2 Department of Physics, Rutgers University, Camden, NJ, USA

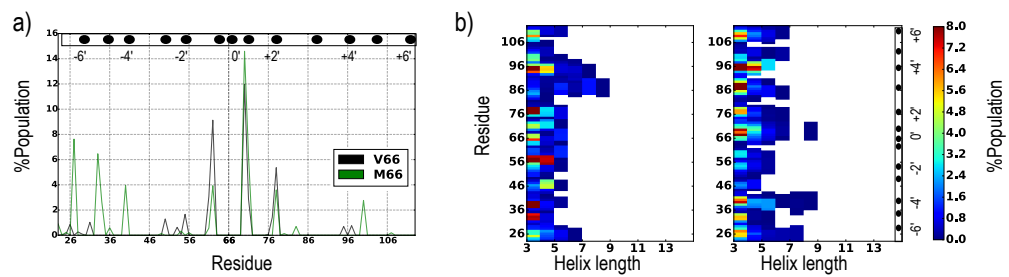
* grace.brannigan@rutgers.edu



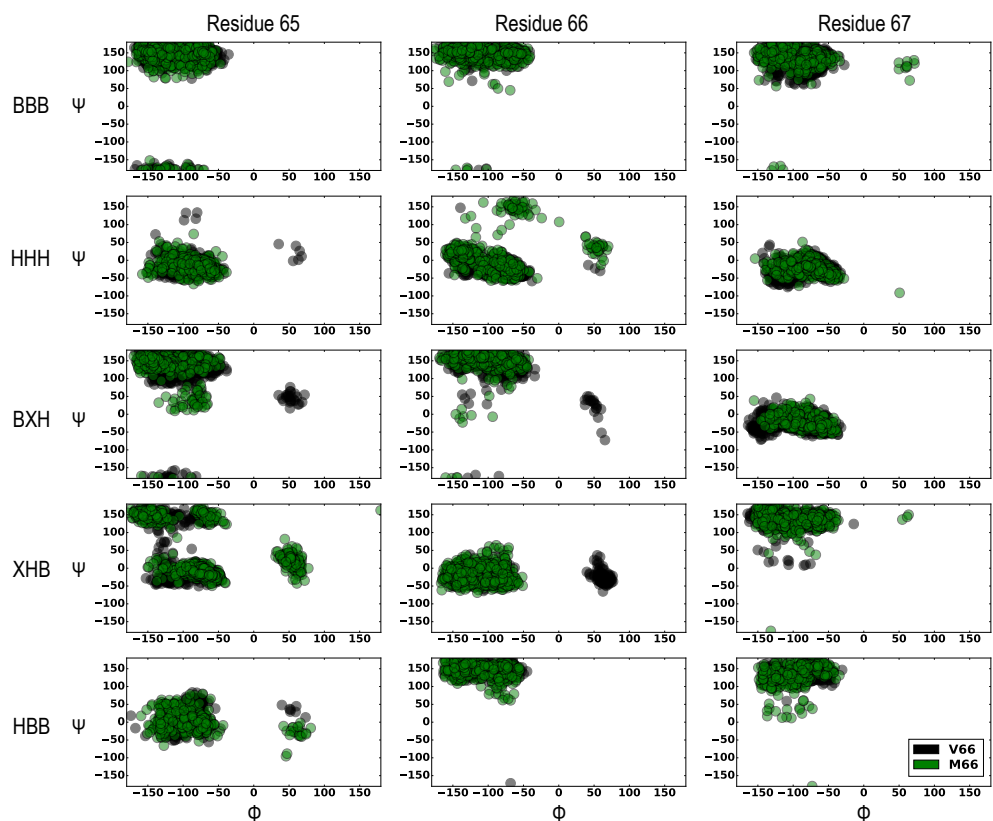
S1 Fig. Mixing of replicas during the simulation. a) Mean square displacement (MSD) of each replica in the temperature range (300K-420K) for both V66 and M66. Replicas visiting 300K are colored green and remaining replicas are colored red. b) Population of each replica at 300K. c) Number of round trips completed by each replica.



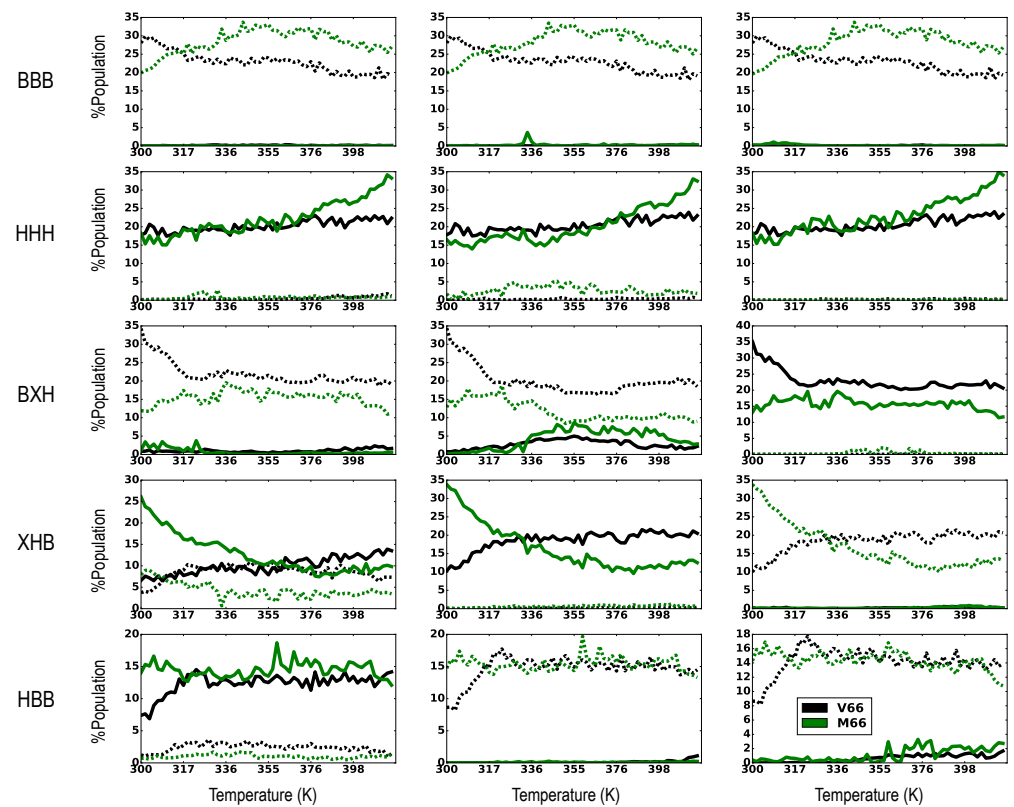
S2 Fig. Temperature dependence of helical length around residue 66. a) Helical propensity at residues 50-77, determined from STRIDE, for helix of length 10,11 and 12 containing residue 66, with curves colored according to temperature. M66 folds into a 12 residue helix at residues 62-74 at high temperature. Representative conformations are shown, colored by secondary structure, with residue 66 in stick representation. b) Total number of replicas at which lengths for helices containing residue 66 is observed, for a range of temperatures. The helices of longer lengths are formed in 4 or more replicas at high temperatures.



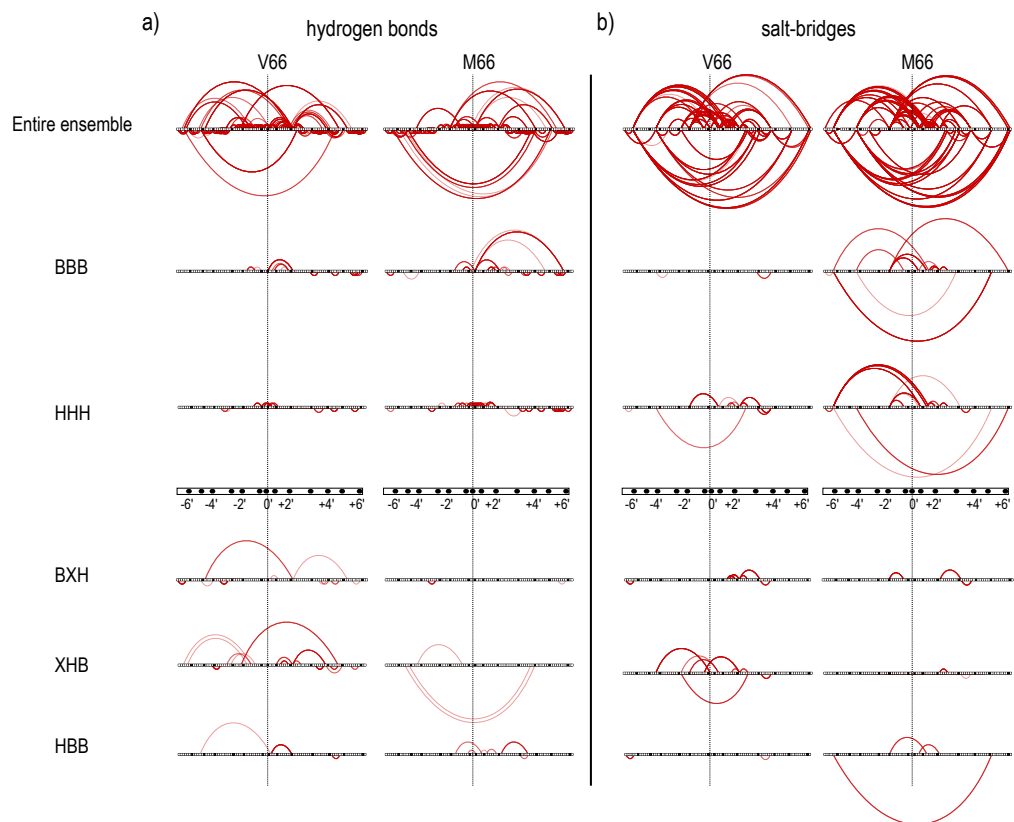
S3 Fig. Backbone hydrogen bonding partners of residue 66 and length of beta sheet formed at every residue at 300K . a) Population of backbone hydrogen bonding of residue 66 with all other residues in the sequence. Residue 66 forms a weak contact with residue at +4' region b) Length of beta strands formed at each residue. Pairing regions show higher density of beta of length 3 or more for both V66 and M66. The strand length formed at each residue was calculated by determining the number of consecutive residues in which the dihedral angles satisfied $\psi > 50^\circ$ and $\phi < -90^\circ$ or $\psi < -120^\circ$ and $\phi < -90^\circ$.



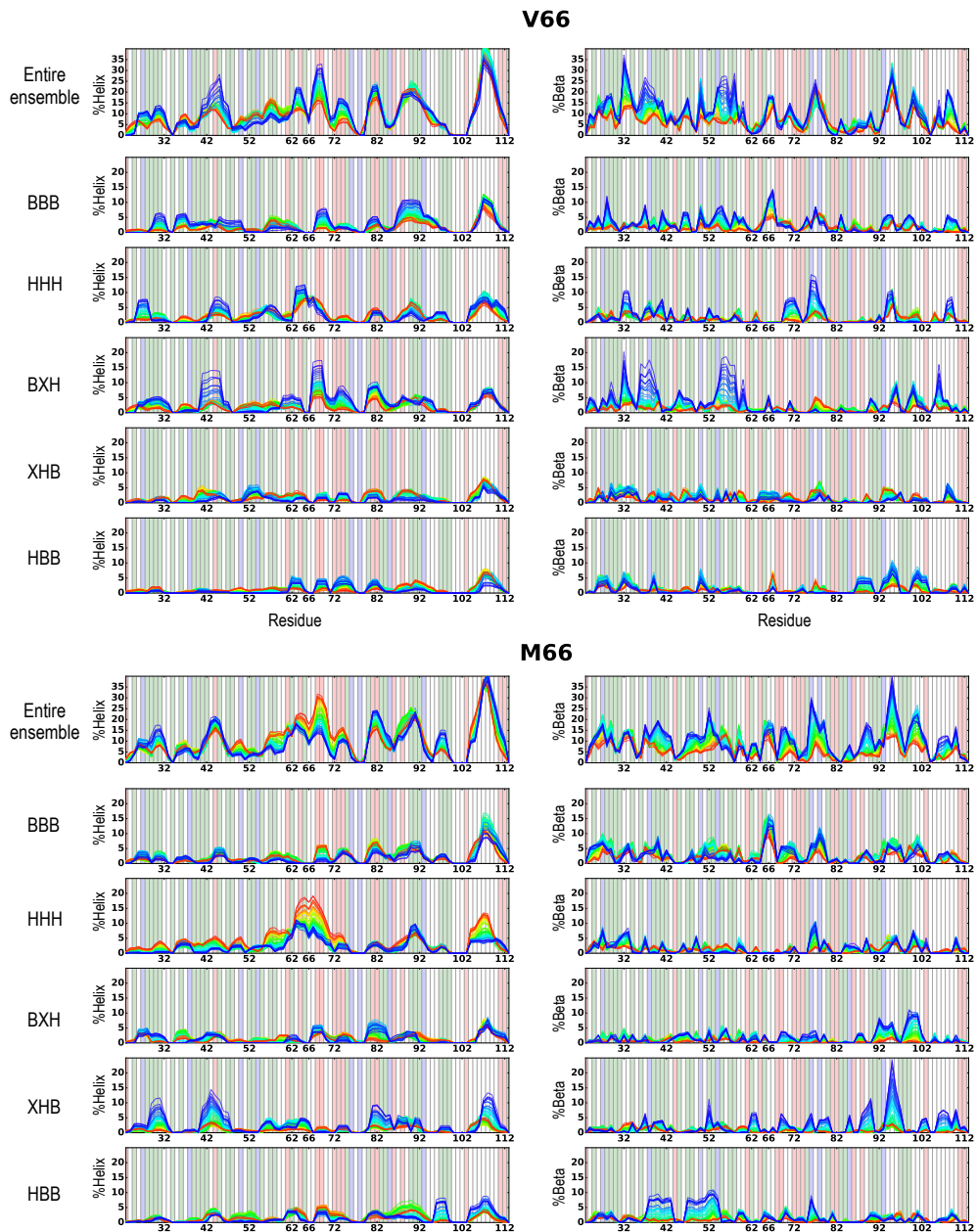
S4 Fig. Distribution of dihedral angles at residue 65,66 and 67 for each cluster at 300K.



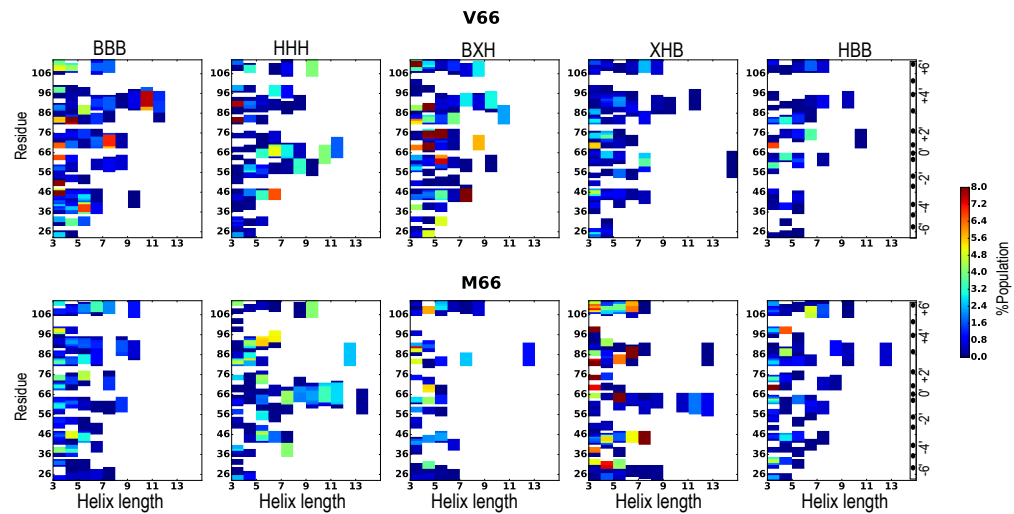
S5 Fig. Distribution of dihedral angles with temperature at residue 65,66 and 67 at each cluster. Dotted lines correspond to $-120^\circ < \psi < 50^\circ$.



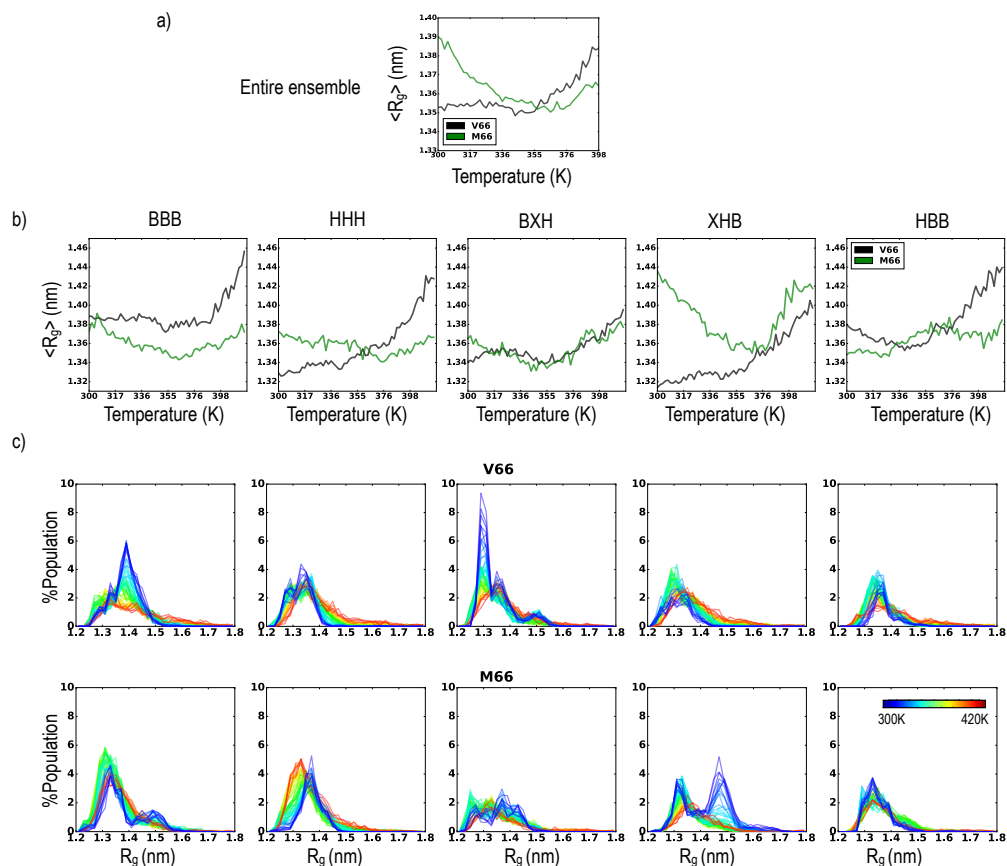
S6 Fig. Linear networks of transient tertiary contacts a) Hydrogen-bonding and b) salt-bridging pairs are shown for the entire ensemble and then decomposed by cluster at high temperatures (398K-420K). The backbone tertiary-contact network is made for V66 and M66, with each residue serving as a node in the network, as described in Methods. Residues at the pairing regions are colored black. Backbone interactions serve as edges between individual network nodes; the thickness of the edge corresponds to the strength of the hydrogen bond, and the transparency of the edge increases as its frequency increases. If residue 66 or its nearby residues (A51-P79) are involved in hydrogen-bond formation then the edge is drawn above the node; otherwise, it is drawn at the bottom of the node. Fewer contact pairs are observed at high temperatures. V66 forms stronger backbone hydrogen-bonding for beta bridge formations and M66 forms stronger backbone hydrogen-bonding for helix formation at residue 66. Cluster HHH in M66 simultaneously forms salt-bridge and hydrogen bonds from residues near the SNP.



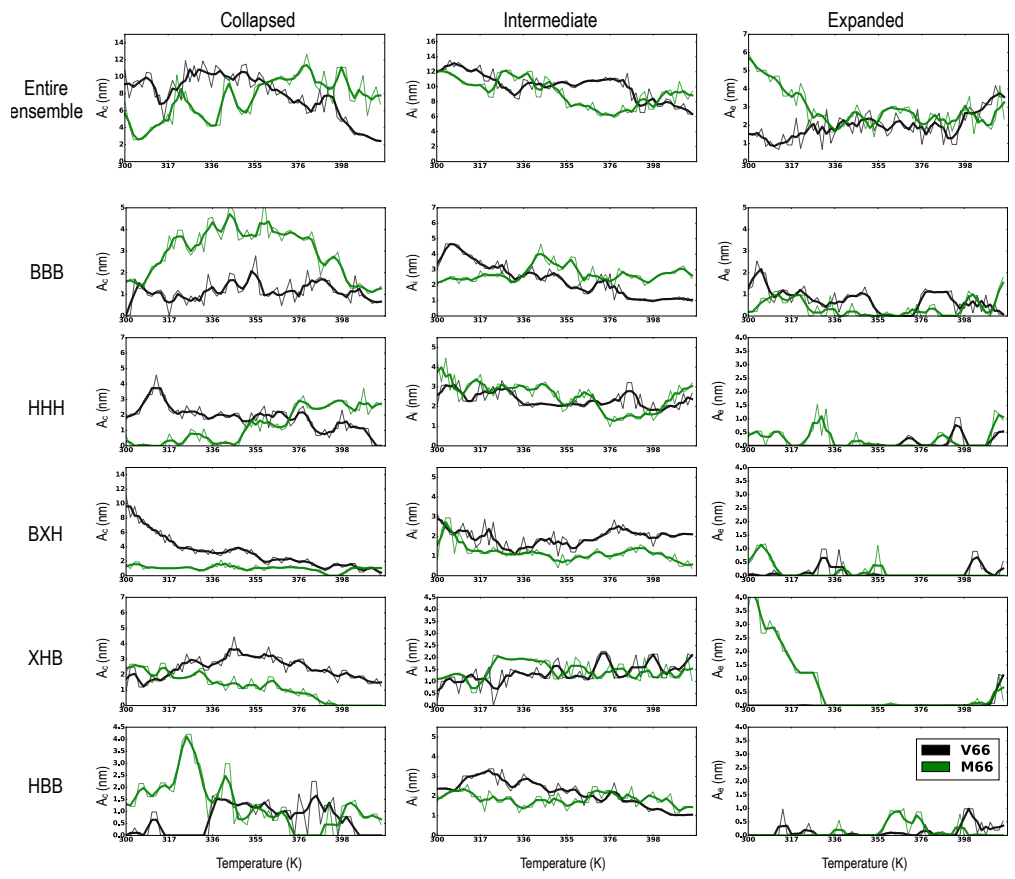
S7 Fig. Secondary structure propensity, determined using STRIDE from MD trajectories, at each residue, with curves colored according to temperature.



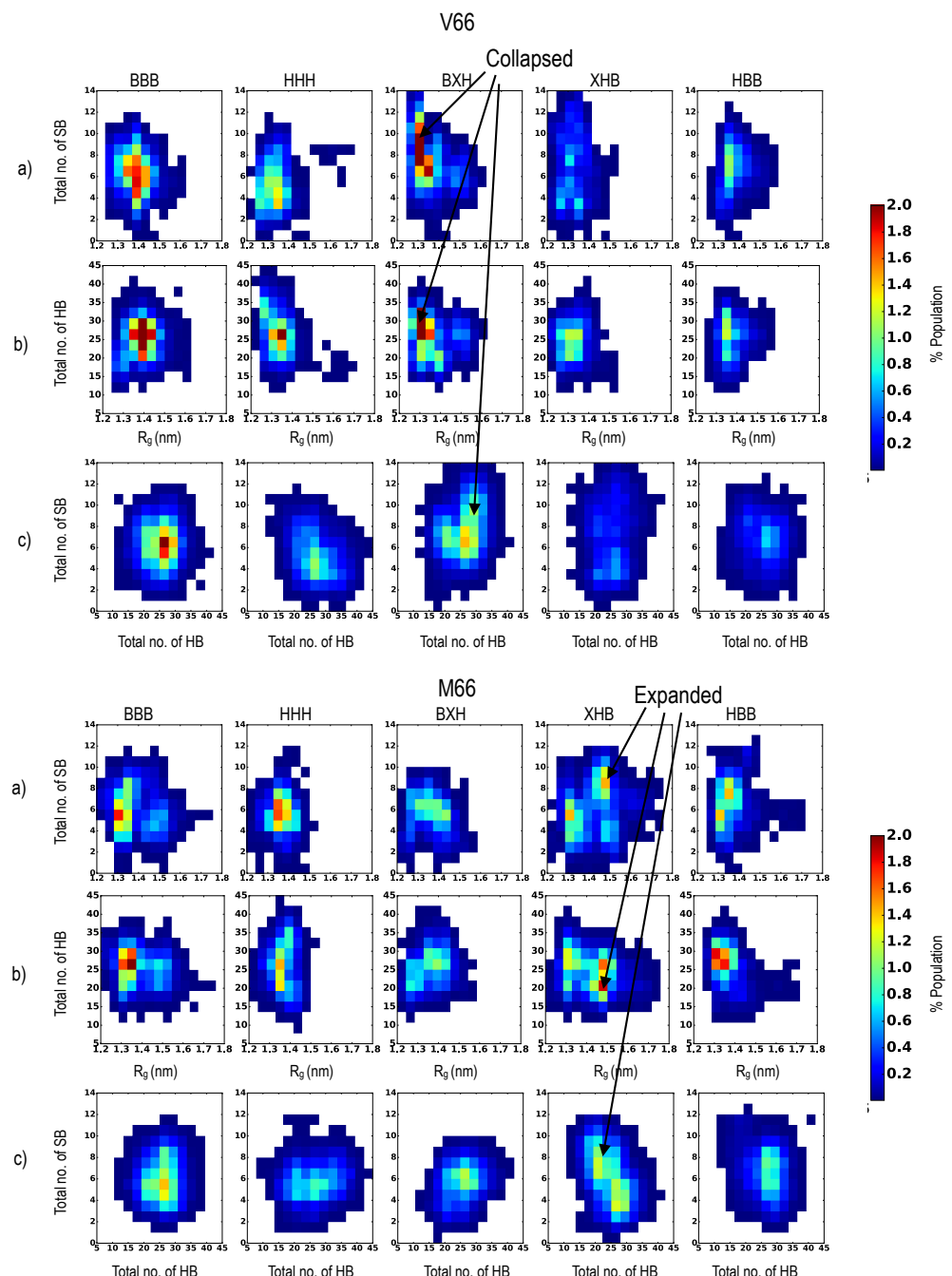
S8 Fig. Length of helix formed at every cluster at 300K. Cluster HHH and Cluster XHB can form long cooperative helices at residue 66. A Smaller helix with 8 or fewer residues forms near residue 66 for clusters BXH,BBB and HBB.



S9 Fig. Distribution of R_g for each cluster. $\langle R_g \rangle$ with temperature for a) entire ensemble and b) each cluster. The $\langle R_g \rangle$ for V66 and M66 reverses with increase in temperature. We observe the same trend reversal for cluster HHH. c) Distribution of R_g for each cluster at every temperature. The line color transitions from blue (cold) to red (hot) with increase in temperature from 300K to 420K.



S10 Fig. Distribution of amplitude of the fitted gaussian curves with temperature. Cluster BXH and XHB shows high amplitude of collapsed and expanded states, respectively at 300K. Cluster HHH shows increase in amplitude for collapsed structure at high temperature.



S11 Fig. Population densities of salt bridges and hydrogen bonds for V66 and M66 for each cluster at low temperatures (300K-317K). Simultaneous salt bridge and hydrogen bonds formation stabilize cluster BXH and only salt bridge formation destabilize cluster XHB. a) Population densities of total number of salt bridges per frame vs R_g (normalized with respect to total number of frames). b) Population densities of total number of hydrogen bonds per frame vs R_g (normalized with respect to total number of frames). c) Population densities of total number of salt bridge per frame vs total number of hydrogen bonds per frame (normalized with respect to total number of frames)